# EFFECTIVE DYNAMICS OF DISCLINATION PAIRS

NICOLÒ BRIATICO †, PIERLUIGI CESANA‡, AND MARCO MORANDOTTI †

Abstract. The dissipative dynamics of a pair of wedge disclinations with opposite Frank angles confined to a circular domain is investigated under the assumption of radially symmetric motion. Two distinct dynamical regimes are identified: a diverging-disclination regime and an annihilating-dipole regime. The stationary points associated with both regimes are determined and fully characterized in terms of their stability, and quantitative estimates for the characteristic evolution times in their vicinity are derived. In the annihilating-dipole regime, it is shown that, after a suitable time rescaling, the resulting law of motion for the dipole coincides with that of an edge dislocation.

## Contents

1. Introduction 1
2. Mechanical model 3
3. Dissipative dynamics 4
4. Stability of the dynamics 7
4.1. Diverging disclinations regime 10
4.2. Converging disclinations regime 11
5. Macroscopic time rescaling and effective dynamics 12
6. Numerical solutions and phase diagram 14
References 17

## 1. Introduction

Dislocations and disclinations (both referred to as defects in this paper, with some abuse of terminology) were introduced by Vito Volterra as prototypical singularities arising from the violation of geometric compatibility in elastic bodies, in planar elasticity [38]. In continuum elasticity, disclinations correspond to violations of rotational symmetry and are characterized by their Frank angle, measuring the angular mismatch, and store large, although finite, elastic energies on bounded domains. Their associated stresses and strains are

*Date*: August 12, 2026.

2020 *Mathematics Subject Classification.* 37N15 (70G75, 74B05, 74H55) .

*Key words and phrases.* Wedge disclinations, disclination dynamics, material defects, dynamical Eshelby equivalence, edge dislocations.

† Dipartimento di Scienze Matematiche "G. L. Lagrange", Politecnico di Torino, Corso Duca degli Abruzzi, 24, 10129 Torino, Italy (nicolo.briatico@polito.it, marco.morandotti@polito.it).

‡ Institute of Mathematics for Industry, Kyushu University, 744 Motooka, Fukuoka, 819-0395, Japan (cesana@math.kyushu-u.ac.jp).

singular, yet square-integrable. Dislocations, on the other hand, are genuine topological singularities carrying a topological charge, and are characterized by the nano-scale Burgers vector. In the classical continuum description, they possess singular energies due to non-integrable stresses and strains. From a mathematical viewpoint, dislocations share important similarities with Ginzburg–Landau vortices and with point charges in two-dimensional Coulomb gases, since all involve long-range logarithmic interactions between topological or effective charges [4, 32].

Because of their distinct energetic and topological nature, the modeling of systems containing both dislocations and disclinations remains challenging. Indeed, dislocations have infinite elastic energy in the continuum limit, while disclinations have finite but size-dependent energy, which complicates the superposition of their respective fields. Nevertheless, Volterra's construction shows that both dislocations and disclinations arise naturally as equilibrium configurations in planar linear elasticity under incompatible kinematics. Thus, they represent fundamental defect structures, both theoretically predicted and experimentally observed [6, 18, 21, 25, 26, 27, 31, 35].

A key structural link between these defects was identified by Eshelby, who observed that the elastic field of an edge dislocation can be represented, at the level of kinematics, as that of a dipole of wedge disclinations, provided a precise relation holds between Burgers vector, Frank angle, and dipole geometry [20]. This observation reveals that dislocations can be viewed as a singular limiting configuration of disclination dipoles. Building on this idea, a variational framework coupling dislocations and disclinations was developed in [14] within linearized elasticity, formulated in terms of the Airy stress function. In particular, it was shown that an edge dislocation can be obtained as the variational limit of a shrinking dipole of wedge disclinations, both at the level of minimizers and minimal energies in static regimes.

When investigating the effects that the presence of these defects has on the material properties, it is fundamental to study their motion, as it has been proved that dislocation motion is linked to plasticity and hardening phenomena [29, 30, 34]. While dislocation dynamics has been extensively studied in both inertial and dissipative settings (see, *e.g.*, [7, 8, 19, 33]), comparatively little is known about the dynamics of disclinations. Recent work [15] introduced and analyzed a dissipative model for finite systems of wedge disclinations, obtaining existence results together with a description of collision times and dipole interactions. However, several fundamental questions remain open, including the analysis of disclination dipoles in their natural scaling regime, the connection with dislocation dynamics, and the renormalization of the associated time-dependent models. For related approaches and models, see [1, 2, 3, 22, 36, 37, 39, 40, 5, 16].

In this work, we study dissipative dynamics of a pair of wedge disclinations with opposite Frank angles. Such configurations naturally screen each other's elastic fields and exhibit two distinct behaviors: when the defects are sufficiently close, they attract and may annihilate, whereas for larger separations they drift toward the boundary and are eventually expelled. Previous work [15] considered mainly symmetric configurations in circular domains. Here we

extend the analysis to asymmetric settings and investigate the fine structure of the dynamics.

After introducing the variational model based on the Airy stress function (Section 2) and a dissipative gradient-flow structure (Section 3), we study the evolution of a pair of disclinations under radial motion from general initial configurations (Section 4). We identify two regimes depending on the initial separation: a diverging regime and a converging regime. In the diverging regime, the defects migrate toward the boundary and behave as isolated disclinations (Section 4.1). In the converging regime (Section 4.2), corresponding to a disclination dipole, the dynamics exhibits a strong separation of time scales: the midpoint evolves slowly, while the inter-defect distance evolves rapidly. Exploiting this behavior, we derive a reduced effective dynamics, and show that it coincides, in the sense of Eshelby's dipole construction, with the dynamics of an edge dislocation located at the center of the dipole (Section 5). Finally, we complement the analytical results with numerical simulations and phase diagrams computed in MATLAB (Section 6).

## 2. Mechanical model

Let $B_R = B_R(0) \subset \mathbb{R}^2$ be the open disk of radius $R > 0$ centered at the origin; we interpret it as the cross-section of an infinite cylinder containing line defects parallel to its axis. Introducing the Young's modulus $E > 0$, the Poisson's ratio $\nu \in (-1, \frac{1}{2})$, and the Airy stress function $v \in H^2(B_R)$, the linearized elastic energy is defined as

$$\mathcal{G}(v; B_R) \coloneqq \frac{1}{2}\frac{1+\nu}{E}\int_{B_R} \left(|\nabla^2 v|^2 - \nu\,(\Delta v)^2\right) \mathrm{d}x.$$

The two isolated disclinations in $B_R$ are modeled through a superposition of Dirac masses supported at the defects locations $y^1, y^2 \in B_R$; more precisely, we introduce the *disclination measure*

$$\theta \coloneqq s_1\,\delta_{y^1} + s_2\,\delta_{y^2},$$

where the $s_k$'s are the associated Frank angles. We combine the elastic energy $\mathcal{G}$ and the measure $\theta$ into the functional introduced in [14, Formula (2.1)]

$$\mathcal{I}^\theta(v; B_R) \coloneqq \frac{1}{2}\frac{1+\nu}{E}\int_{B_R} \left(|\nabla^2 v|^2 - \nu\,(\Delta v)^2\right) \mathrm{d}x + s_1 v(y^1) + s_2 v(y^2),$$

where the last two summands are the explicit expression of the duality $\langle \theta, v\rangle$. The corresponding Euler–Lagrange equation under traction-free boundary conditions reads

$$\begin{cases} \dfrac{1-\nu^2}{E}\,\Delta^2 v = -\theta & \text{in } B_R, \\ \nabla^2 v\, t = 0 & \text{on } \partial B_R, \end{cases} \tag{1}$$

and it has been shown in [14, Proposition 1.10] that

$$\nabla^2 v\, t = 0 \quad \text{on } \partial B_R \quad \text{if and only if} \quad v = a, \quad \partial_n v = \partial_n a \quad \text{on } \partial B_R,$$

for some affine function $a\colon \mathbb{R}^2 \to \mathbb{R}$. Since affine functions are in the kernel of the operators appearing in (1), without loss of generality we can choose

$a = 0$, thus reducing the traction-free boundary conditions to homogeneous boundary condition. The differential problem in (1) now reads

$$\begin{cases} \dfrac{1-\nu^2}{E}\,\Delta^2 v = -\theta & \text{in } B_R\,, \\ v = \partial_n v = 0 & \text{on } \partial B_R\,, \end{cases} \tag{2}$$

which is the Euler–Lagrange equation associated with the minimization problem

$$\min\{\mathcal{I}^\theta(v; B_R) : v \in H^2_0(B_R)\}. \tag{3}$$

In the same spirit as [15], letting $\bar{v}$ be the unique solution to (3), by Clapeyron's theorem, the minimal elastic energy can be expressed by

$$\mathcal{G}(\bar{v}; B_R) = -\frac{1}{2}\langle \theta, \bar{v}\rangle = -\frac{1}{2}\big(s_1\bar{v}(y^1) + s_2\bar{v}(y^2)\big) =: \mathcal{W}(y^1, y^2; B_R). \tag{4}$$

The solution $\bar{v}$ corresponds to that of the *clamped disk problem* (2) and it can be expressed via the associated Green's function, see, *e.g.*, [28]. In particular, the solution reads

$$\bar{v}(x) = \sum_{k=1}^{2} \bar{v}^k(x),$$

where the functions $\bar{v}^k \colon B_R \to \mathbb{R}$ are defined by

$$\begin{aligned} \bar{v}^k(x) = -CR^2 s_k \Bigg[ \frac{|x-y^k|^2}{R^2} \log\!\left(\frac{|x-y^k|^2}{R^2}\right) + \left(1 - \frac{|x|^2}{R^2}\right)\left(1 - \frac{|y^k|^2}{R^2}\right) \\ - \frac{|x-y^k|^2}{R^2} \log\!\left(\frac{R^4 - 2R^2 x\cdot y^k + |x|^2|y^k|^2}{R^4}\right)\Bigg], \end{aligned}$$

if $x \neq y^k$, and are extended by continuity to $x = y^k$, with $\bar{v}^k(y^k) = -CR^2 s_k\Big(1 - \frac{|y^k|^2}{R^2}\Big)^2$, where we introduce the constant

$$C := \frac{E}{1-\nu^2}\frac{1}{16\pi}$$

collecting the mechanical parameters. The function $\mathcal{W}(\cdot,\cdot; B_R)\colon B_R \times B_R \to \mathbb{R}$ provides the value of the minimal elastic energy at the equilibrium as a function of the positions of the disclinations, and is particularly suited to study their dissipative dynamics.

## 3. Dissipative dynamics

In this section, we derive the equations of motion for a pair of disclinations with opposite Frank angle

$$s_1 = -s_2 =: s > 0. \tag{5}$$

In this context, the total Frank angle vanishes in $B_R$, but if the two disclinations get arbitrarily close, then, upon suitably rescaling by the dipole length, the resulting system is kinematically and energetically equivalent to an edge dislocation (see, *e.g.* [14, 20]). In particular, the Burgers vector of the resulting edge dislocation has magnitude $s$ and points in the direction which is the $\pi/2$-rotation of that from $y^2$ to $y^1$, see [14, page 88].

With our choice of Frank angles (5), the explicit expression of the minimal elastic energy (4) is

$$\begin{aligned}\mathcal{W}(y^1,y^2;B_R) =& \frac{1}{2}CR^2s^2\Bigg[\left(1-\frac{|y^1|^2}{R^2}\right)^2+\left(1-\frac{|y^2|^2}{R^2}\right)^2\\ &-2\left(1-\frac{|y^1|^2}{R^2}\right)\left(1-\frac{|y^2|^2}{R^2}\right)\\ &+2\frac{|y^2-y^1|^2}{R^2}\log\left(\frac{R^4-2R^2y^1\cdot y^2+|y^1|^2|y^2|^2}{R^2|y^2-y^1|^2}\right)\Bigg],\end{aligned} \tag{6}$$

and, under the assumption that disclinations evolve according to the *maximal dissipation criterion* [12, 13, 15, 24], the velocity of each defect is proportional to the steepest descent of the minimal elastic energy. This leads to the following system of ODEs:

$$\begin{cases}\dot{y}^k(t) = -\lambda_k\nabla_{y^k}\mathcal{W}(y^1,y^2;B_R), & \text{for } t>0,\\ y^k(0) = y^{k,0}\in B_R\,,\end{cases} \tag{7}$$

for $k=1,2$. The parameters $\lambda_k$ appearing above are a mobility parameters with units $[\lambda_k]=[\mathrm{s\,kg^{-1}}]$. Various mobility functions are known for screw dislocations, see, *e.g.*, [9, 10, 11, 12]; here, we focus only on the isotropic case and therefore we consider $\lambda_1=\lambda_2=\lambda\in\mathbb{R}$.

By observing that the energy $\mathcal{W}$ in (6) rescales quadratically in $R$ by passing from $B_1$ to $B_R$, namely

$$\mathcal{W}(Ry^1,Ry^2;B_R) = R^2\mathcal{W}(y^1,y^2;B_1), \qquad \text{for } y^1,y^2\in B_1\,,$$

following [15, Section 3.1], it is convenient to recast (7) in non-dimensional form. By means of the rescaling

$$\frac{y^k}{R}\mapsto y^k \quad\text{and}\quad C\lambda t\mapsto t, \tag{8}$$

and by defining $W(\cdot,\cdot)\colon B_1\times B_1\to\mathbb{R}$ as

$$W(y^1,y^2) := \frac{1}{CR^2}\mathcal{W}(Ry^1,Ry^2;B_R), \qquad \text{for } y^1,y^2\in B_1,$$

system (7) becomes, for $k=1,2$,

$$\begin{cases}\dot{y}^k(t) = -\nabla_{y^k}W(y^1,y^2), & \text{for } t>0,\\ y^k(0) = y^{k,0}\in B_1\,.\end{cases} \tag{9}$$

We will focus on an arrangement of disclinations $y^1=(y^1_1,y^1_2), y^2=(y^2_1,y^2_2)\in B_1$ located on a diameter, which they never abandon by symmetry reasons. Therefore, if $y^{1,0}_2=y^{2,0}_2=0$ and $y^{1,0}_1>y^{2,0}_1$, then it is not restrictive to consider that $y^1_2(t)=y^2_2(t)=0$ and $y^1_1(t)>y^2_1(t)$ for every $t>0$. The ordering $y^1_1>y^2_1$ is maintained throughout the evolution since collision of disclinations occurs in infinite time (see, *e.g.*, [15, Section 3.3.1], where the study is conducted for the even more symmetric case $y^{1,0}_1=-y^{2,0}_1$). Owing to these considerations, it is convenient to introduce the new variables

$$\begin{aligned}h(t) &= h\big(y^1(t),y^2(t)\big) := |y^1(t)-y^2(t)| = y^1_1(t)-y^2_1(t),\\ d(t) &= d\big(y^1(t),y^2(t)\big) := \frac{1}{2}\big(y^1_1(t)+y^2_1(t)\big),\end{aligned}$$

which describe the disclination separation (dipole length, if it is very small) and the midpoint of the pair (center of the dipole, if $h$ is very small), respectively. The relationship

$$y^k(t) = d(t) + \frac{(-1)^{k+1}}{2} h(t), \qquad \text{for } k = 1, 2, \tag{10}$$

returns the positions of the disclinations starting from the center and the inter-disclination distance.

The dynamics is defined for $y_1^1 \in (-1, 1)$ and $y_1^2 \in (-1, y_1^1)$ and it corresponds in a one-to-one fashion, to $d \in (-1, 1)$ and $h \in (0, 2)$ with the constraint that $d \pm \frac{1}{2}h \in (-1, 1)$. Should $d$ be negative, we could switch signs to $y_1^1$, $y_1^2$ and $s$, and bring ourselves back to the situation where $d \geq 0$. Therefore, the dynamics for the pair $(h, d)$ is considered in the set

$$\mathcal{R} := \left\{ (h, d) \in (0, 2) \times [0, 1) \colon 0 < d + \frac{h}{2} < 1 \right\},$$

and it is determined, from (9), by

$$\begin{cases} \dot{h} = 4s^2 h \left[ 2 \log\left( \dfrac{4h}{4 - 4d^2 + h^2} \right) + \dfrac{4 - 4d^2 - h^2}{4 - 4d^2 + h^2} - 2d^2 \right] =: f(h, d), \\ \dot{d} = \dfrac{2s^2 h^2 d\,(4d^2 - h^2)}{4 - 4d^2 + h^2} =: g(h, d), \\ h(0) = y_1^{1,0} - y_1^{2,0} =: h_0 \in (0, 2), \\ d(0) = \frac{1}{2}\left(y_1^{1,0} + y_1^{2,0}\right) =: d_0 \in [0, 1), \end{cases} \tag{11}$$

with the constraint that $(h_0, d_0) \in \mathcal{R}$.

System (11) can more conveniently be re-written by introducing $\zeta \colon [0, +\infty) \to \mathbb{R}^2$ defined by $t \mapsto \zeta(t) := (h(t), d(t))$, and the vector field $\Phi \colon \overline{\mathcal{R}} \to \mathbb{R}^2$ defined by $\Phi(h, d) := (f(h, d), g(h, d))$ in $\mathcal{R}$, and extended by continuity on $\partial\mathcal{R}$ by

$$\begin{cases} \Phi(0, d) = (0, 0), \\ \Phi\left(h, 1 - \dfrac{h}{2}\right) = \big( -2s^2 h\,(1 - h)(2 - h), s^2 h\,(1 - h)(2 - h) \big). \end{cases} \tag{12}$$

Thus, the dynamics (11) can be extended to

$$\begin{cases} \dot{\zeta} = \Phi(\zeta), \\ \zeta(0) = (h_0\,, d_0) =: \zeta_0 \in \overline{\mathcal{R}}. \end{cases} \tag{13}$$

The next result ensures that the dynamics (13) is well posed for any initial datum $\zeta_0 \in \overline{\mathcal{R}} \setminus \mathcal{L}$, where $\mathcal{L} := \partial\overline{\mathcal{R}} \cap \{h = 0\}$. Notice that the case in which $\zeta_0 \in \mathcal{R}$ describes a physical situation with both disclinations inside the domain $B_1$; the case in which $\zeta_0 = (h_0, 1 - h_0/2)$ for $h_0 \in (0, 2)$, corresponds to the case of $y_1^1 = 1 \in \partial B_1$ and $y_1^2 \in (-1, 1)$, the disclination $y^1$ sitting at the boundary and the disclination $y^2$ being alone in the domain. As we will see, when one disclination is at the boundary, it does not affect the dynamics of the remaining one. Yet, considering this case is necessary to establish the well-posedness result (see Theorem 3.1 below).

The case in which $\zeta_0 = (0, d_0)$, for a certain $d_0 \in [0, 1]$ will be commented on in Remark 3.2 below.

**Theorem 3.1.** *For any initial datum $\zeta_0 \in \overline{\mathcal{R}} \setminus \mathcal{L}$, problem (13) admits a unique solution $\zeta \in C^1([0,+\infty); \overline{\mathcal{R}} \setminus \mathcal{L})$, satisfying $\zeta(0) = \zeta_0$ .*

*Proof.* We start by observing that $\Phi$ is locally Lipschitz-continuous on $\overline{\mathcal{R}} \setminus \mathcal{L}$. Therefore, by standard results on ODE theory, for every choice of $\zeta_0 \in \overline{\mathcal{R}} \setminus \mathcal{L}$, there exists a unique local solution to (13).

If $\zeta_0 = (h_0, 0)$, for some $h_0 \in (0,2)$, then the dynamics is defined for all $t > 0$ and, in this case, $d(t) = 0$. This corresponds to the case of $y^1(t) = -y^2(t)$ for every $t > 0$ and it has been thoroughly studied in [15, Section 3.3].

If $\zeta_0 = (h_0, 1 - h_0/2)$, for some $h_0 \in (0,2)$, then the dynamics corresponds to an initial condition for which the disclination $y^1$ starts off at the boundary of the domain and the disclination $y^2$ starts off in the interior of $B_1$ . In this situation, since

$$\frac{g(h, 1-h/2)}{f(h, 1-h/2)} = -\frac{1}{2},$$

the dynamics is confined to the edge $\{(h,d) = (h, 1-h/2)\}$, so that $y^1$ neither moves nor influences the dynamics of $y^2$, which, in turn, behaves as the only defect in the domain. The resulting equation of motion for $y^2 =: \eta$ is

$$\dot{\eta} = 2s^2\eta(1-\eta^2), \qquad \eta_0 = 1 - h_0 \in (-1,1), \tag{14}$$

which is well defined for all $t > 0$, and is the same that has been found and studied in [15, Section 3.2].

If $\zeta_0 \in \operatorname{int} \mathcal{R}$, then the maximal solution is defined for $t \in [0,+\infty)$ and is confined in $\operatorname{int} \mathcal{R}$. Indeed, if there existed a time $\tilde{t}$ such that $\zeta(\tilde{t}) \in \{d = 0\} \cup \{(h, 1-h/2)\}$, then uniqueness of the solution of the two previous cases would be violated. □

**Remark 3.2.** *We notice that $\Phi$ loses Lipschitz continuity on $\{h = 0\}$, so that uniqueness is not guaranteed there. Yet, if $\zeta_0 = (0, d_0)$, then $\zeta(t) = (0, d_0)$ for every $t > 0$ is a constant solution, see (12); on the other hand, if $\zeta_0 \in \mathcal{R}$, then the velocity field $\Phi$ becomes infinitesimal in a right neighborhood of $\mathcal{L}$, suggesting that solutions can hit the boundary segment $\{h = 0\}$ in infinite time. As a matter of fact, we will prove this in Proposition 4.7, and this corresponds to the two disclinations colliding. This behavior is very interesting for us. Indeed, in [14] it has been proved that upon rescaling by (the square of) the separation distance, a colliding dipole of disclinations is energetically equivalent to an edge dislocation. Therefore, this suggests that when $t \mapsto h(t)$ vanishes, the dynamics $t \mapsto d(t)$ of the center of the dipole converges, after a suitable time rescaling, to that of an edge dislocation; see Section 5.*

## 4. Stability of the dynamics

In this section, we study the equilibria of (13). We will identify three isolated equilibrium points and we will single out the boundary segment $\mathcal{L}$ as made of equilibrium points, and we discuss their stability and their mechanical interpretation.

Moreover, we find that there are two regimes for the pair of disclinations, namely one in which it breaks and the two defects move away from one another

($\zeta(+\infty) = (2,0)$, discussed in Section 4.1), and one in which the dipole collides ($\zeta(+\infty) = (0, d_\infty)$, for some $d_\infty \in (0,1)$, discussed in Section 4.2).

We recall that an *equilibrium point* for system (13) is a point $\zeta_* \in \overline{\mathcal{R}}$ such that $\Phi(\zeta_*) = (0,0)$. Moreover, we say that an equilibrium point $\zeta_* \in \overline{\mathcal{R}}$ is *locally asymptotically stable* if there exists a neighborhood $\mathcal{N}$ of $\zeta_*$ in $\overline{\mathcal{R}}$ such that for every initial condition $\zeta_0 \in \mathcal{N}$, the corresponding solution $\zeta$ to (13) satisfies that $\lim_{t\to+\infty} \zeta(t) = \zeta_*$. We say that an equilibrium point $\zeta_* \in \overline{\mathcal{R}}$ is *unstable* if the dynamics associated with an initial condition $\zeta_0$ close to $\zeta_*$ grows far from $\zeta_*$.

One way to deduce the asymptotic stability of an equilibrium point $\zeta_*$ is to study the linearization of (13) at $\zeta_*$: if the Jacobian matrix $J\Phi(\zeta_*)$ has (complex) eigenvalues with negative real part, then $\zeta_*$ is (locally) asymptotically stable (see, *e.g.*, [23]).

We now characterize the set

$$\mathcal{Z}_\Phi := \big\{(h,d) \in \overline{\mathcal{R}} : \Phi(h,d) = (0,0)\big\} = \mathcal{Z}_f \cap \mathcal{Z}_g$$

of equilibria of (13), where

$$\mathcal{Z}_f := \mathcal{A} \cup \mathcal{L} \cup \{(2,0)\} \quad \text{and} \quad \mathcal{Z}_g := \mathcal{B} \cup \mathcal{L} \cup \mathcal{S}. \tag{15}$$

In (15), $\mathcal{A}$ is the arc along which $\tilde{f}(h,d) := f(h,d)/4s^2h$ vanishes; $\mathcal{B} = \{(h,0), h \in [0,2]\}$, and $\mathcal{S} = \{(h, h/2), h \in [0,1]\}$. Thus,

$$\mathcal{Z}_\Phi = \mathcal{L} \cup \{E_1, E_2, E_3\},$$

the three isolated points being

$$E_1 := (h_*, 0), \qquad E_2 := (1, \tfrac{1}{2}), \qquad E_3 := (2,0),$$

where $h_* \approx 0.8$ is the unique root of the function $f$ restricted to $\operatorname{int}\mathcal{B}$, namely of the function $h \mapsto f(h,0)$ for $h \in (0,2)$.

**Remark 4.1.** *The point $E_1$ corresponds to the symmetric arrangement $y_1^1 = -y_1^2 \approx 0.4$, which was found in* [15, Section 3.3.1] *(where our $h_*$ corresponds to $\Delta_{\mathrm{eq}}$) as the stationary configuration of a disclination pair placed symmetrically with respect to the center of the disk.*

*The point $E_2 \in \{(h, 1-h/2)\} \cap \partial\mathcal{R}$ is the configuration where the disclination $y^1$ lies on the boundary, while the disclination $y^2$ sits at the center of the domain. This corresponds to the equilibrium point $\eta = 0$ for the corresponding dynamics (14), which is that of an isolated disclination in $B_1$, see* [15, Section 3.2]. *Following the same interpretation, the point $E_3$ corresponds to the limiting situation of both disclinations $y^1$ and $y^2$ being located at antipodal points of $\partial B_1$. Notice that $E_3$ corresponds to the equilibrium point $\eta = -1$ for (14). In this case, no dynamics occurs.*

The following proposition characterizes the nature of the isolated equilibrium points $E_i$, $i = 1,2,3$.

**Proposition 4.2** (Characterization of the stationary configurations)**.** *Let $E_i$, $i = 1,2,3$, be the isolated equilibrium points of (13). Then $E_1$ and $E_2$ are unstable equilibria and $E_3$ is a locally asymptotically stable equilibrium.*

*Proof.* By computing the Jacobian matrix of the vector field $\Phi$ and evaluating it at the points $E_i$, $i = 1, 2, 3$, we find

$$J\Phi(E_1) = \begin{pmatrix} \dfrac{256s^2}{(4+h_*^2)^2} - 8s^2 & 0 \\ 0 & -\dfrac{2h_*^4 s^2}{4+h_*^2} \end{pmatrix},$$

which is already diagonal and with negative determinant, thus $E_1$ is unstable; the eigenvalues of

$$J\Phi(E_2) = \begin{pmatrix} s^2 & -2s^2 \\ -s^2/2 & s^2 \end{pmatrix},$$

are 0 and $2s^2$, so that $E_2$ is unstable; finally $J\Phi(E_3) = -4s^2 I_{2\times 2}$ proves the local asymptotic stability of $E_3$. □

To study the dynamics out of these equilibrium points, as well as to investigate the stability of the set $\mathcal{L}$, it is convenient to single out the following three regions contained in $\operatorname{int}\mathcal{R}$ (see Figure 1):

$$\begin{aligned} \mathcal{R}_1 &:= \big\{(h,d) \in \overline{\mathcal{R}} \colon f(h,d) < 0 \text{ and } g(h,d) > 0\big\}, \\ \mathcal{R}_2 &:= \big\{(h,d) \in \overline{\mathcal{R}} \colon f(h,d) < 0 \text{ and } g(h,d) < 0\big\}, \\ \mathcal{R}_3 &:= \big\{(h,d) \in \overline{\mathcal{R}} \colon f(h,d) > 0 \text{ and } g(h,d) < 0\big\}. \end{aligned}$$

We notice that $\mathcal{A} = \partial\mathcal{R}_2 \cap \partial\mathcal{R}_3$ and that $\mathcal{S} = \partial\mathcal{R}_1 \cap \partial\mathcal{R}_2$.

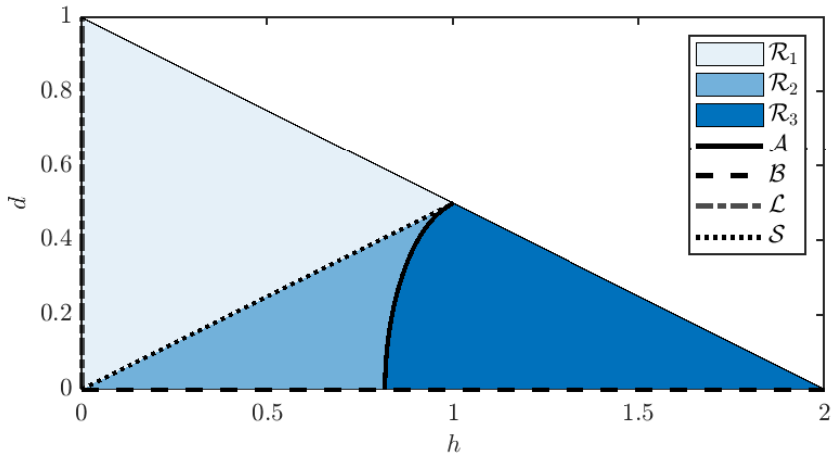



FIGURE 1. Plot of the regions $\mathcal{R}_i$, $i = 1, 2, 3$.

We will prove that if $\zeta_0 \in \overline{\mathcal{R}}_3 \setminus \{E_1, E_2\}$, then the dynamics will converge to $E_3$ (see Proposition 4.4), whereas, if $\zeta_0 \in \overline{\mathcal{R}_1 \cup \mathcal{R}_2} \setminus \mathcal{A}$, then the dynamics will converge to a point in $\mathcal{L}$ (see, Proposition 4.7). In other terms, the arc $\mathcal{A}$ divides the dynamics of the pair in a diverging regime, characterized by $\zeta(+\infty) = E_3$, and in a converging regime, characterized, instead, by $\zeta(+\infty) \in \mathcal{L}$.

4.1. **Diverging disclinations regime.** We now analyse the region where the disclinations move toward the boundary along opposite direction. In the $(h, d)$ plane, this is equivalent to proving that the dynamics tends to the equilibrium point $E_3$.

We start by proving a structural property of the arc $\mathcal{A}_*$, with $\mathcal{A}_* := \mathcal{A} \setminus \{E_1, E_2\}$, namely that it is the graph of a function.

**Lemma 4.3.** *There exists a strictly increasing function $d_{\mathcal{A}_*}\colon (h_*, 1) \to (0, 1/2)$ such that $\mathcal{A}_* = \mathrm{graph}(d_{\mathcal{A}_*}) = \{(h, d) \in \mathcal{R} : h \in (h_*, 1), d = d_{\mathcal{A}_*}(h)\}$.*

*Proof.* The result follows from an application of the Implicit Function Theorem. Indeed, it is easy to verify that $\partial_d \tilde{f}(h, d) < 0$ for every $(h, d) \in \mathcal{A}_*$. Therefore, the condition $\tilde{f}(h, d) = 0$ can be inverted on $\mathcal{A}_*$ and this proves that there exists $d_{\mathcal{A}_*}\colon (h_*, 1) \to (0, 1/2)$ such that $\mathcal{A}_* = \mathrm{graph}(d_{\mathcal{A}_*})$. The strict monotonicity of $d_{\mathcal{A}_*}$ follows from implicit differentiation:

$$d'_{\mathcal{A}_*}(h) = -\frac{\partial_h \tilde{f}(h, d_{\mathcal{A}_*}(h))}{\partial_d \tilde{f}(h, d_{\mathcal{A}_*}(h))},$$

and an explicit verification shows that $d'_{\mathcal{A}_*}(h) > 0$ for every $h \in (h_*, 1)$. □

We are now ready to prove the main result in this section.

**Proposition 4.4** (Diverging regime)**.** *For every $\zeta_0 \in \overline{\mathcal{R}}_3 \setminus \{E_1, E_2\}$, the unique solution to (13) is such that*

$$\lim_{t \to +\infty} \zeta(t) = E_3\,. \tag{16}$$

*Proof.* Owing to Theorem 3.1, the dynamics (13) is well posed. By Lemma 4.3, if $\zeta_0 \in \mathcal{A}_*$, then $\dot{\zeta}(0) = \Phi(\zeta_0) = (0, g(h_0, d_0))$, with $g(h_0, d_0) < 0$. Thus, $\zeta(t)$ enters the region $\mathrm{int}\,\mathcal{R}_3$ as soon as $t$ is positive. Once $\zeta(\bar{t}) \in \mathcal{R}_3$ for a certain $\bar{t} \geq 0$, then $\zeta(t) \in \mathcal{R}_3$ for every $t \geq \bar{t}$. By uniqueness and by the monotonicity of the components of $\Phi$ in $\mathcal{R}_3$, (16) follows. □

**Remark 4.5.** *Reading Proposition 4.4 for the dynamics of the two disclinations yields that, for large times, they behave as two isolated defects, whose motion is only due to the attraction to the boundary. Indeed, by considering the leading order of (13) for $\zeta \to E_3$, i.e., $h \to 2$ and $d \to 0$, we have (see (11))*

$$\begin{cases} \dot{h} = 4s^2(2 - h) \\ \dot{d} = -4s^2 d \\ h(0) = h_0\,,\ d(0) = d_0 \end{cases}$$

*(we can assume $d_0 \ll 1$ without loss of generality), whose solution is*

$$h(t) = 2 - (2 - h_0)\exp(-4s^2 t), \quad \text{and} \quad d(t) = d_0 \exp(-4s^2 t).$$

*Recalling (10), one immediately sees that the dynamics of the defects is*

$$y^k(t) = (-1)^{k+1} - ((-1)^{k+1} - y^{k,0})\exp(-4s^2 t),$$

*which is consistent with the results in* [15, Section 3.2]*, where an isolated disclination tends to the boundary of the domain.*

4.2. **Converging disclinations regime.** Let us focus on the region where the disclination pair tends to collapse, namely when $\zeta \to (0, d_\infty) \in \mathcal{L}$ for some $d_\infty \in [0,1]$ as $t \to +\infty$.

We start by proving the following proposition, which, in the language of dynamical systems, states that the line $\mathcal{L}$ is the $\omega-$limit set of the region $\overline{\mathcal{R}_1 \cup \mathcal{R}_2} \setminus \mathcal{A}$.

**Proposition 4.6.** *For any initial datum $\zeta_0 \in \overline{\mathcal{R}_1 \cup \mathcal{R}_2} \setminus \mathcal{A}$, the corresponding unique solution to (13) is such that $\zeta(+\infty) \in \mathcal{L}$.*

*Proof.* By Theorem 3.1, the solution to (13) is well defined for all positive times and is confined in the region $\mathcal{R}$. Since $\zeta_0$ is not in the basin of attraction of the equilibrium point $E_3$ (see Proposition 4.4), $\zeta(+\infty) \neq E_3$. If $\zeta(+\infty) = \bar{\zeta} \in \mathcal{R}_1 \cup \mathcal{R}_2$, this would mean that there exists an asymptotically stable equilibrium in the interior of $\mathcal{R}$, contradicting our previous analysis. Therefore, it must be that $\zeta(+\infty) \in \mathcal{L}$. □

In view of Proposition 4.6, we now focus on a right neighbourhood $U_0 \subset \mathcal{R}_1$ (to be specified presently) of $\mathcal{L}$. In $U_0$, since $h \approx 0$, we may analyze system (13) by considering only the leading order in $h$ for each variable, namely

$$\begin{cases} \dot{h} = 8s^2 h \log \dfrac{h}{1-d^2} =: \varphi(h,d)\,, \\ \dot{d} = 2s^2 h^2 \dfrac{d^3}{1-d^2} =: \gamma(h,d)\,, \\ h(0) = h_0,\ d(0) = d_0\,, \end{cases} \tag{17}$$

with $\zeta_0 = (h_0, d_0) \in U_0$. System (17) cannot be integrated explicitly, yet existence and uniqueness of solutions to the Cauchy problem can be obtained by an application of the standard results from ODE theory. In the regime $h \approx 0$, the asymptotic dynamics in (17) exhibits a fast-slow structure. Indeed, $\gamma$ is negligible with respect to $\varphi$ as $h \to 0$, determining that $d$ evolves on a slower time scale than $h$.

In view of the increasing monotonic behavior and the concavity of the curve of $h \mapsto d(h)$,[1] we can estimate that $d_\infty \in (d_0, d_{\max})$, where

$$d_{\max} := d_0\Big(1 - \frac{h_0^2 d_0^2}{4(1-d_0^2)\log(h_0/(1-d_0^2))}\Big)\,,$$

and corresponds to the evolution along the tangent line with slope determined by the initial conditions, namely $\gamma(\zeta_0)/\varphi(\zeta_0)$ (see Figure 2).

From the explicit expression of $d_{\max}$ the region $U_0$ can be determined as the one where the initial condition $\zeta_0$ satisfies:

$$\zeta_0 \in \mathcal{R}_1\,, \quad h_0 < 1 - d_{\max}^2\,, \quad \text{and} \quad d_{\max} < 1.$$

We are now ready to prove the main result of this section.

**Proposition 4.7** (Converging regime)**.** *Under the same assumption of Proposition 4.6, the unique solution to (13) is such that $h \in L^2(\mathbb{R}^+)$.*

[1] As a consequence of the Implicit Function Theorem, we have that

$$\frac{\mathrm{d}^2(d(h))}{\mathrm{d}h^2} = \frac{\mathrm{d}}{\mathrm{d}h}\Big(\frac{\gamma(h,d(h))}{\varphi(h,d(h))}\Big) = \frac{d^3}{4(1-d^2)\log(h/(1-d^2))} + o(h), \qquad \text{as } h \to 0,$$

which is, to leading order in $h$, negative.

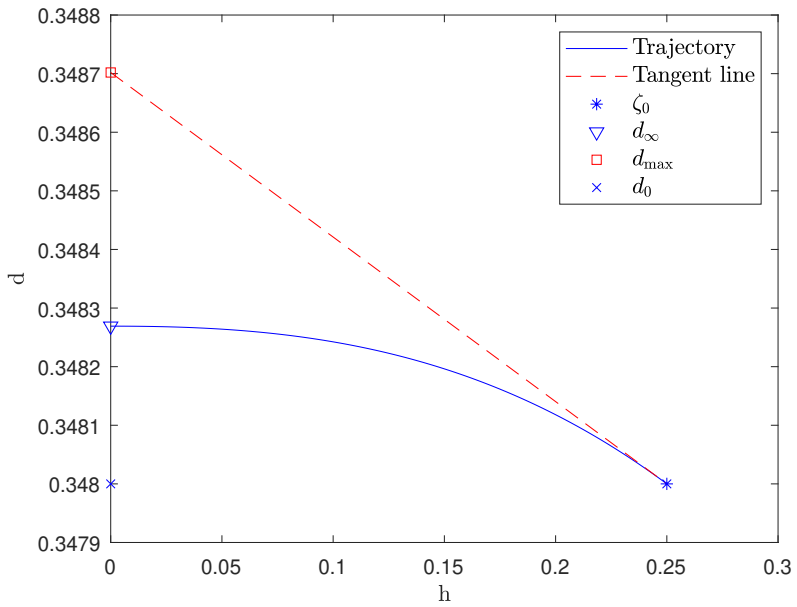



FIGURE 2. Plot of the trajectory $h \mapsto d(h)$ (blue line), and its tangent line (red dotted line).

*Proof.* As a consequence of Proposition 4.6, for every $\zeta_0 \in \mathcal{R}_1 \cup \mathcal{S} \cup \mathcal{R}_2$ there exists a time $t^* \geq 0$ such that $\zeta(t^*) \in U_0$, where we can use (17), up to restarting the dynamics and setting $t^* = 0$. In particular, due to the monotonicity of the dynamics (in $U_0$, $h$ is strictly decreasing and $d$ is strictly increasing), and that of $\varphi$ with respect to $d$, we deduce that

$$\varphi(h, d_0) \leq \varphi(h, d) \leq \varphi(h, d_{\max}).$$

By comparison, it follows that $h_\ell(t) \leq h(t) \leq h_{\mathrm{u}}(t)$, for every $t > 0$, where $h_\ell$ and $h_{\mathrm{u}}$ are the solutions to

$$\begin{cases} \dot{h} = \varphi(h, d_0), \\ h(0) = h_0 \end{cases} \qquad \text{and} \qquad \begin{cases} \dot{h} = \varphi(h, d_{\max}), \\ h(0) = h_0 \end{cases}$$

respectively, whose explicit solutions are

$$\begin{aligned} h_\ell(t) =& (1 - d_0^2) \exp\left( \log \frac{h_0}{1 - d_0^2} \cdot \exp(8s^2 t) \right), \\ h_{\mathrm{u}}(t) =& (1 - d_{\max}^2) \exp\left( \log \frac{h_0}{1 - d_{\max}^2} \cdot \exp(8s^2 t) \right). \end{aligned}$$

Since both $\log(h_0/(1 - d_0^2))$ and $\log(h_0/(1 - d_{\max}^2))$ are negative in $U_0$, it follows that $h_\ell, h_{\mathrm{u}} \in L^2(\mathbb{R}^+)$, and the thesis follows by comparison. □

## 5. Macroscopic time rescaling and effective dynamics

Motivated by the equivalence between an edge dislocation and a collapsing disclination dipole, first identified at the kinematic level by Eshelby [20] and subsequently established at the energetic level in [14], we show that the

dynamics of the dipole center is governed by the same evolution law as that of an edge dislocation. This extends the equivalence to the dynamical setting.

This is obtained by a suitable time rescaling, that is necessary because of the separation of time scales in (17).

By reformulating the dynamics according to the time rescaling (18), the collision of the dipole now occurs in finite time. This behavior is analogous, at least heuristically, to that observed for dislocations. In Remark 5.2 we comment that this analogy is in fact exact. We point out that the $L^2$ integrability of $h$ plays a crucial role here.

**Theorem 5.1** (Effective dislocation dynamics)**.** *Let $\zeta_0 \in U_0$ and let $t \mapsto h(t)$ be the associated solution to the Cauchy problem (17). Let $\tau\colon \mathbb{R}^+ \to \mathbb{R}^+$ be (the macroscopic time) defined as*

$$\tau(t) \coloneqq \frac{1}{2}\int_0^t h^2(s)\,\mathrm{d}s. \tag{18}$$

*Then the function $\tau$ is invertible and the rescaled dynamics of $d$ as a function of $\tau$, namely $\delta(\tau) \coloneqq d(\sigma(\tau))$ ($\sigma$ being the inverse function of $\tau$) satisfies*

$$\log\Big(\frac{\delta^2}{{\delta_0}^2}\Big) + \frac{1}{\delta^2} - \frac{1}{\delta_0^2} + 8s^2\tau = 0. \tag{19}$$

*Moreover, $\delta$ collides with the boundary of the domain in finite time.*

*Proof.* The function $\tau$ defined in (18) has the following properties: $\tau(0) = 0$, it is strictly increasing, and

$$\tau_\infty \coloneqq \lim_{t\to+\infty} \tau(t) = \frac{1}{2}\int_0^{+\infty} h^2(s)\,\mathrm{d}s \in \mathbb{R}^+,$$

owing to the fact that $h \in L^2(\mathbb{R}^+)$ (see Proposition 4.7).

The inverse function $\sigma$ is therefore defined from the interval $[0, \tau_\infty]$ to $\mathbb{R}^+$, and allows us to define the rescaled dynamics of the centre of the dipole via $\delta(\tau) = d(\sigma(\tau))$. By the chain rule, the dynamics for $d$ in (17) reads now

$$\begin{cases} \delta'(\tau) = 4s^2\dfrac{\delta^3(\tau)}{1-\delta^2(\tau)} & \text{for } \tau \in (0, \tau_\infty], \\ \delta(0) = \delta_0 \coloneqq d_0\,. \end{cases} \tag{20}$$

By separation of variables, the solution to (20) is given by (19). Moreover, since $\delta'(\tau) > 0$ for all $\tau$, the motion occurs towards the boundary and the time needed to reach it ($\delta = 1$) is

$$\bar\tau = \frac{1}{8s^2}\left(\log {\delta_0}^2 - 1 + \frac{1}{{\delta_0}^2}\right). \qquad \square$$

**Remark 5.2.** *The time rescaling introduced by (18) allows us to appreciate the dynamics of the $d$ variable, which is much slower than that of the dipole length $h$ in (17). In particular, owing to the introduction of the macroscopic time $\tau$ and by recasting the dynamics of $d$ in (17) as in (20), we see that the equation for $\delta$ coincides with that of a collapsing dipole of disclinations found in* [17, Section 3.2].

*There, the dipole length $h$ is treated as a small parameter that converges to zero. Here, on the contrary, the function $t \mapsto h(t)$ is a solution to the*

*dynamics. In the converging disclinations regime treated in Section 4.2, it vanishes. This suggests the question whether these two limiting cases may lead to the same mechanical behaviour. Theorem 5.1 proves that the two resulting dynamics (that is* [17, Section 3.2] *and that in* (20)*) are the same.*

*This may be thought of as a dynamical version of Eshelby equivalence: a moving colliding dipole of disclinations generates a moving edge dislocation. Moreover, if this dislocation is not placed at the center of the disk (as is our case), then it is attracted to the boundary and collides on it in finite time (see also* [24, Section 4.2] *for the analogous case of a screw dislocation).*

## 6. Numerical solutions and phase diagram

In this section, we describe some numerical experiments that we ran to clarify the dynamics in $\mathcal{R}$. Let us consider the time interval $[0, T]$, for some $T > 0$. Given $N \in \mathbb{N} \setminus \{0\}$ and $n \in \{0, \dots, N\}$, we define

$$\Delta t := \frac{T}{N}, \qquad \text{and} \qquad t_n := n\Delta t = \frac{n}{N}T$$

and then introduce

$$h^n := h(t_n) \qquad \text{and} \qquad d^n := d(t_n),$$

with $h^0 = h_0$ and $d^0 = d_0$. Therefore, the time-discrete version of system (13) in terms of $\zeta^n = (h^n, d^n)$ reads

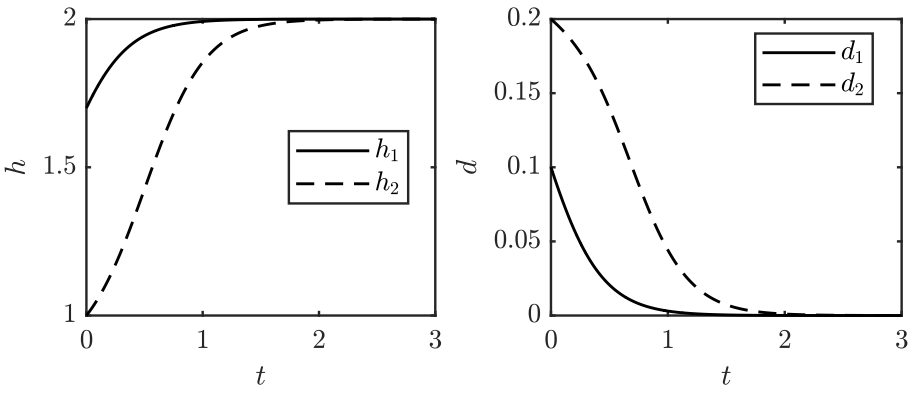
$$\zeta^n = \zeta^{n-1} + \Delta t\, \Phi(\zeta^{n-1}), \qquad \text{with } \zeta^0 = (h_0, d_0),$$

which can be solved via the explicit Euler scheme. We implemented our own formulation of the explicit Euler method and run it in the MATLAB R2026b environment.

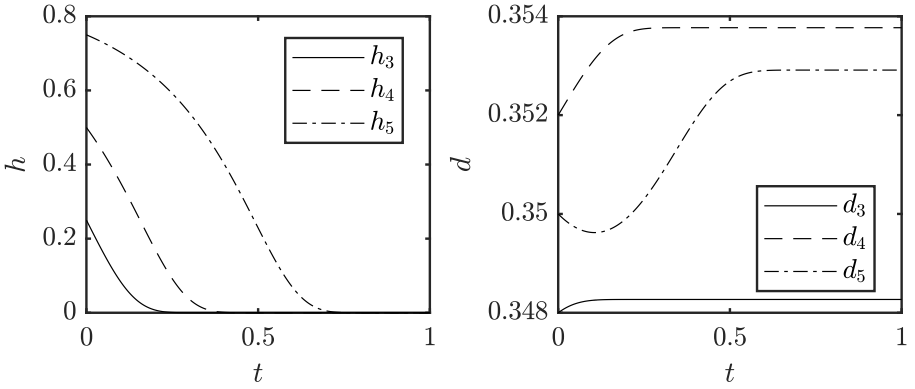
We consider different initial configurations, in order to capture the emergence of the possible behaviors of a pair of disclinations arranged radially. The results of the simulations are shown in Figure 3 and are divided into diverging (on the top) and converging (on the bottom) regimes.

As pointed out in [15, Section 3.1], the dynamics of disclinations is the result of the interplay of three factors: (i) the presence of the boundary, (ii) the disclination-boundary interaction, and (iii) the pairwise interactions between disclinations. The identification of these three different contributions provides a useful tool for understanding the numerical simulations. In particular, the diverging regime simulations reveal two qualitatively different scenarios. Referring to the top row of Figure 3, in the $(h_1, d_1)$ scenario, the monotonicity and the concavity properties of the trajectories of $h$ and $d$ suggest that the boundary effects dominate the evolution. On the other hand, in the $(h_2, d_2)$ scenario, the change in concavity observed in both trajectories indicates an initial competition between the mutual disclination interaction and the boundary contribution.

By contrast, the converging regime is characterized by three qualitatively different scenarios. In the $(h_3, d_3)$ scenario, the monotonicity and the concavity properties of the trajectories of $h$ and $d$ indicate that the mutual disclination interaction is dominant; while, in the $(h_4, d_4)$ scenario, the monotonicity and the change in concavity observed in both trajectories suggest an initial competition between the mutual disclination interaction and the




(A) Diverging regime




(B) Converging regime

FIGURE 3. Possible scenarios of the dynamics of the pair of disclinations. On the top, the diverging regime characterized by $h \to 2$ and $d \to 0$. On the bottom, the converging regime characterized by $h \to 0$ and $d \to d_\infty$ .

boundary contribution. Finally, in the $(h_5, d_5)$ scenario, the behavior of the trajectories (in particular that of $d$) suggests an initial balance between the mutual disclination interaction and the boundary contribution, which in the end evolves as in the $(h_3, d_3)$ scenario.

We conclude this section by constructing a map that associates to each initial point $\zeta_0 = (h_0, d_0) \in \overline{\mathcal{R}} \setminus \mathcal{L}$ the final point $\zeta_{\text{end}} = (h_{\text{end}}, d_{\text{end}}) \in \overline{\mathcal{R}} \setminus \mathcal{L}$ determined by numerically solving (13) up to a time $\overline{T} > 0$. The phase diagram in Figure 4 (top picture) is constructed by choosing $\overline{T} = 20$ and $N = 10^6$.

We classify each initial point $\zeta_0$ in the domain in terms of its final state $\zeta_{\text{end}}$.

Investigation of the numerical solutions confirm the emergence of the three main regimes analyzed: converging regime, diverging regime, and stationary regime. In particular,

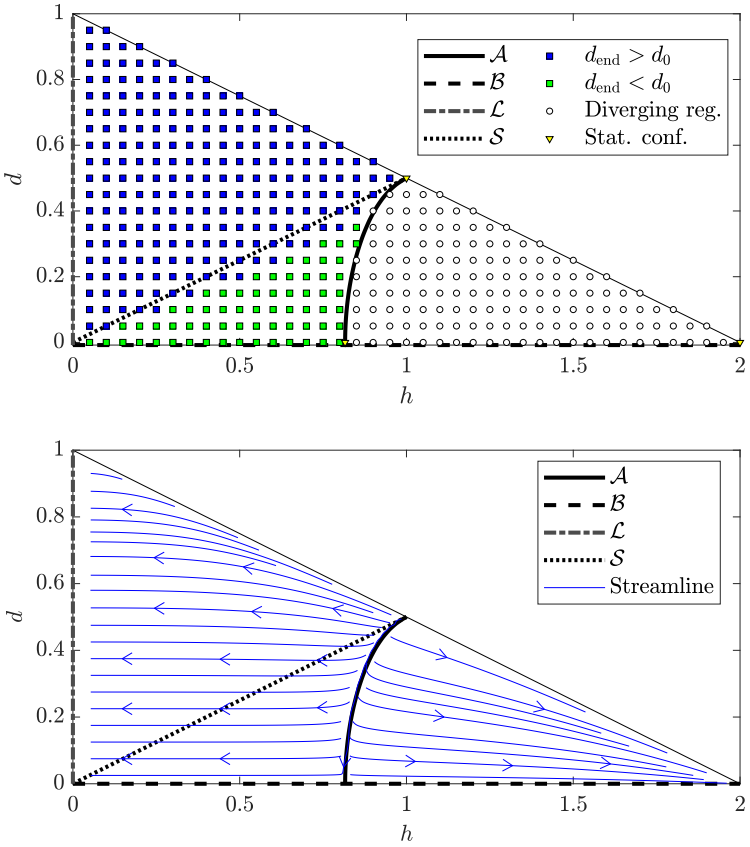



FIGURE 4. On the top, the phase diagram of the disclination dynamics. Here squares correspond to initial configurations in the colliding dipole regime while circles indicate initial configurations in the diverging disclination regimes. On the bottom, the flux lines plotted with the *streamslice* native Matlab function.

- The filled square represents the converging behavior: the defects are converging to $(0, d_{\text{end}}) \in \mathcal{L}$ for some point $d_{\text{end}} \in [0, 1]$. Blue squares indicate that the final position of the midpoint of the dipole has increased compared to the initial position ($d_{\text{end}} > d_0$), while green squares show that the midpoint of the dipole has decreased ($d_{\text{end}} < d_0$).
- The circle represents the diverging behavior: the two defects are far enough not to experience the presence of the other defect and therefore, each one behaves as an isolated disclination and tends to reach the boundary of the domain ($h \to 2$, $d \to 0$).
- The triangle represents the stationary points. In particular, we note that, for the sake of completeness, we manually added the initial configuration sample the stationary configuration $E_1$.

Finally, we complete the phase diagram by using the Matlab native function *streamslice* to draw the flux lines of the problem. Figure 4 (bottom picture)

clearly shows that the arc $\mathcal{A}$ is the border between the converging and the diverging regime.

**Acknowledgements**. JASSO scholarship offered within the "Kyushu University Program for Emerging Leaders in Science" (Q-PELS) and local support received at the Institute of Mathematics for Industry, an international Joint Usage and Research facility located at Kyushu University (NB). PC's work is supported by JSPS KAKENHI Grant-in-Aid for Scientific Research (C) JP24K06797. MM acknowledges partial support from the MUR grant Geometric Analytic Methods for PDEs and Applications (2022SLTHCE cup E53D23005880006). This manuscript reflects only the authors' views and opinions and the Italian Ministry cannot be considered responsible for them. PC holds an honorary appointment at La Trobe University. NB, PC, and MM are members of the Gruppo Nazionale per l'Analisi Matematica, la Probabilità e le loro Applicazioni (GNAMPA) of the Istituto Nazionale di Alta Matematica (INdAM). MM and NB thank the Institute of Mathematics for Industry, an International Joint Usage and Research Center located in Kyushu University; PC thanks the Department of Mathematical Sciences "G. L. Lagrange" of Politecnico di Torino where part of the work contained in this paper was carried out.

## References

[1] A. Acharya. A model of crystal plasticity based on the theory of continuously distributed dislocations. *Journal of the Mechanics and Physics of Solids*, 49(4):761–784, 2001.

[2] A. Acharya. New inroads in an old subject: Plasticity, from around the atomic to the macroscopic scale. *Journal of the Mechanics and Physics of Solids*, 58(5):766–778, 2010.

[3] A. Acharya and C. Fressengeas. Continuum mechanics of the interaction of phase boundaries and dislocations in solids. In G.-Q. G. Chen, M. Grinfeld, and R. J. Knops, editors, *Differential Geometry and Continuum Mechanics*, pages 123–165, Cham, 2015. Springer International Publishing.

[4] A. Alastuey and B. Jancovici. On the classical two-dimensional one-component coulomb plasma. *Journal de Physique*, 42(1):1–12, 1981.

[5] J. Ball, P. Cesana, and B. Hambly. A probabilistic model for martensitic avalanches. *MATEC Web of Conferences*, 33, 2015.

[6] F. Banhart, J. Kotakoski, and A. V. Krasheninnikov. Structural defects in graphene. *ACS Nano*, 5(1):26–41, 2011. PMID: 21090760.

[7] E. Bitzek and P. Gumbsch. Atomistic study of drag, surface and inertial effects on edge dislocations in face-centered cubic metals. *Materials Science and Engineering: A*, 387-389:11–15, 2004. 13th International Conference on the Strength of Materials.

[8] E. Bitzek, D. Weygand, and P. Gumbsch. Atomistic study of edge dislocations in fcc metals: Drag and inertial effects. In H. Kitagawa and Y. Shibutani, editors, *IUTAM Symposium on Mesoscopic Dynamics of Fracture Process and Materials Strength*, pages 45–57, Dordrecht, 2004. Springer Netherlands.

[9] T. Blass, I. Fonseca, G. Leoni, and M. Morandotti. Dynamics for systems of screw dislocations. *SIAM Journal on Applied Mathematics*, 75(2):393–419, 2015.

[10] G. A. Bonaschi, P. van Meurs, and M. Morandotti. Dynamics of screw dislocations: a generalised minimising-movements scheme approach. *European Journal of Applied Mathematics*, 28(4):636–655, 2017.

[11] M. Cannone, A. El Hajj, R. Monneau, and F. Ribaud. Global existence for a system of non-linear and non-local transport equations describing the dynamics of dislocation densities. *Archive for Rational Mechanics and Analysis*, 196(1):71–96, 2010.

[12] P. Cermelli and M. E. Gurtin. The motion of screw dislocations in crystalline materials undergoing antiplane shear: glide, cross-slip, fine cross-slip. *Archive for Rational Mechanics and Analysis*, 148(1):3–52, 1999.
[13] P. Cermelli and G. Leoni. Renormalized energy and forces on dislocations. *SIAM Journal on Mathematical Analysis*, 37(4):1131–1160, 2005.
[14] P. Cesana, L. De Luca, and M. Morandotti. Semidiscrete modeling of Systems of Wedge Disclinations and Edge Dislocations via the Airy Stress Function Method. *SIAM J. on Math. Anal.*, 56:79–136, 2024.
[15] P. Cesana, A. Grillo, M. Morandotti, and A. Pastore. Dissipative dynamics of Volterra disclinations. *SIAM J. Appl. Math.*, 85(4):1361–1386, 2025.
[16] P. Cesana and B. Hambly. A probabilistic model for interfaces in a martensitic phase transition. *Journal of Applied Probability*, 2022.
[17] P. Cesana, M. Morandotti, and A. Sambo. Equilibrium and Interaction Regimes in Mixed Disclination-Dislocation Systems. https://arxiv.org/abs/2608.10930, *preprint*, 2026.
[18] P. Cesana, M. Porta, and T. Lookman. Asymptotic analysis of hierarchical martensitic microstructure. *J. of the Mech. and Phys. of Solids*, 72:174–192, 2014.
[19] S. V. Dmitriev, A. A. Nazarova, A. I. Pshenichnyuk, and A. M. Iskandarov. Dynamics of edge dislocation clusters interacting with running acoustic waves. *Discrete and Continuous Dynamical Systems - S*, 4(5):1079–1094, 2011.
[20] J. D. Eshelby. A simple derivation of the elastic field of an edge dislocation. *British Journal of Applied Physics*, 17(9):1131–1135, sep 1966.
[21] D. Essmann and H. Träuble. The Direct Observation of Individual Flux Lines in Type II Superconductors. *Phys. Letters*, 24A(526), 1967.
[22] A. Garroni, P. van Meurs, M. A. Peletier, and L. Scardia. Convergence and non-convergence of many-particle evolutions with multiple signs. *Archive for Rational Mechanics and Analysis*, 235(1):3–49, 2020.
[23] M. W. Hirsch, S. Smale, and R. L. Devaney. *Differential equations, dynamical systems, and an introduction to chaos*. Elsevier/Academic Press, Amsterdam, third edition, 2013.
[24] T. Hudson and M. Morandotti. Properties of screw dislocation dynamics: time estimates on boundary and interior collisions. *SIAM J. Appl. Math.*, 77(5):1678–1705, 2017.
[25] T. Inamura. Geometry of kink microstructure analysed by rank-1 connection. *Acta Materialia*, 173:270–280, 2019.
[26] T. Inamura, H. Hosoda, and S. Miyazaki. Incompatibility and preferred morphology in the self-accommodation microstructure of $\beta$-titanium shape memory alloy. *Philosophical Magazine*, 93(6):618–634, 2013.
[27] T. Inamura, M. Ii, M. Tahara, and H. Hosoda. Formation process of the incompatible martensite microstructure in a beta-titanium shape memory alloy. *Acta Materialia*, 124:351–359, 2017.
[28] M. Nakai and L. Sario. Green's function of the clamped punctured disk. *J. Austral. Math. Soc.*, **20** (Series B):175–181, 1978.
[29] E. Orowan. Zur Kristallplastizität. III. *Z. Physik*, 89:634–659, 1934.
[30] M. Polanyi. Über eine Art Gitterstörung, die einen Kristall plastisch machen könnte. *Z. Physik*, 89:660–664, 1934.
[31] M. Porta and T. Lookman. Heterogeneity and phase transformation in materials: Energy minimization, iterative methods and geometric nonlinearity. *Acta Materialia*, 61(14):5311–5340, 2013.
[32] E. Sandier and S. Serfaty. 2D Coulomb gases and the renormalized energy. *The Annals of Probability*, 43(4):2026–2083, 2015.
[33] Y. Tang. Uncovering the inertia of dislocation motion and negative mechanical response in crystals. *Scientific Reports*, 8(1):140, Jan 2018.
[34] G. I. Taylor. The Mechanism of Plastic Deformation of Crystals. Part I. Theoretical. *Proceedings of the Royal Society of London. Series A*, 145:362–387, 1934.
[35] H. Träuble and D. Essmann. Fehler im Flussliniengitter Von Supraleitern zweiter Art. *Phys Stat Sol*, 25, 1968.

[36] P. van Meurs and M. Morandotti. Discrete-to-continuum limits of particles with an annihilation rule. *SIAM Journal on Applied Mathematics*, 79(5):1940–1966, 2019.

[37] P. van Meurs, M. A. Peletier, and N. Požár. Discrete-to-continuum convergence of charged particles in 1D with annihilation. *Arch. Ration. Mech. Anal.*, 246(1):241–297, 2022.

[38] V. Volterra. Sur l'équilibre des corps élastiques multiplement connexes. *Annales scientifiques de l'École Normale Supérieure*, 24:401–517, 1907.

[39] C. Zhang and A. Acharya. On the relevance of generalized disclinations in defect mechanics. *Journal of the Mechanics and Physics of Solids*, 119:188–223, 2018.

[40] X. Zhang, A. Acharya, N. J. Walkington, and J. Bielak. A single theory for some quasi-static, supersonic, atomic, and tectonic scale applications of dislocations. *Journal of the Mechanics and Physics of Solids*, 84:145–195, 2015.